Electronic Supplementary Material (ESI) for Journal of Materials Chemistry C.

Supplementary Information

Morphology and Polarization-Dependent Second Harmonic Generation in Single Hexagonal Sodium Niobate Micro/Nano-crystal

Quanlan Xiao[1], Wei Lin[1], Gengxu Chen[2], Chengjie Ding[2], Guoping Dong[1,*], Chensheng Lin[3], Botao Wu[2], E Wu[2], Heping Zeng[2] and Jianrong Qiu[1,*]

[1]State Key Laboratory of Luminescent Materials and Devices and Institute of Optical Communication Materials, South China University of Technology, Guangzhou 510640, China

[2]State Key Laboratory of Precision Spectroscopy, East China Normal University, Shanghai 200062, China

[3]State Key Laboratory of Structural Chemistry, Fujian Institute of Research on the Structure of Mater, the Chinese Academy of Sciences, Fuzhou, Fujian 350002, China

* E-mail: dgp@scut.edu.cn; qjr@scut.edu.cn

1 Experimental section

The flowchart for preparing $NaNbO_3$ micro/nano-crystals by a solution-phase ion exchange route is shown in Fig. S1. The experimental parameters of as-prepared $NaNbO_3$ micro/nano-crystals are summarized in Table S1.

1.1 $Nb_2O_5 \cdot nH_2O$ colloid

0.30 g Nb_2O_5 (AR) reacted with melting KOH. Then the resulting product was cooled and dissolved in distilled water, and the colloid of $Nb_2O_5 \cdot nH_2O$ was obtained by adding glacial acetic acid until the solution reached appropriate acidity. The as-prepared products were washed and filtered several times, then used as raw materials for the next experiment.

1.2 Potassium niobate nanoparticles ($KNbO_3$ NPs)

0.60 g NH_4F and 0.90 g $CO(NH_2)_2$ were dissolved in 10 mL distilled water at room temperature, and the as-prepared niobic acid ($Nb_2O_5 \cdot nH_2O$) in the previous step was slowly added to the solution under magnetic stirring. 2.0 mL 30% H_2O_2 and 8.0 mL 1.3 M KOH aqueous solution was then added. The mixture was transferred into a Teflon-lined stainless steel autoclave (50 mL capacity), which was heated at 180℃ for 36 h. The as-prepared products were washed for several times with distilled water. Finally, the sample was dried at 60℃ for 3-5 h in air.

1.3 $NaNbO_3$ micro/nano-crystals

0.12 g $KNbO_3$ NPs were dispersed in 20 mL 1.0 M NaOH aqueous solutions. In order to control the morphology, polyacrylamide (PA), ethyleneglycol (EG), or ethylenediamine (EN) were added to the alkaline solution, respectively (see Table S1). The solution was transferred into a Teflon-lined 50 mL capacity autoclave, which was heated at 180℃ for 36 h. After the autoclave was air-cooled down to room temperature, the powders were collected, rinsed with distilled water, and dried at 60℃ for 3-5 h in air.

1.4 Single $NaNbO_3$ micro/nano-crystals preparation

Starting from a dried powder, we first dispersed $NaNbO_3$ micro/nano-crystals in ethanol (99.7% purity). Then 50 μL of the solution was dropped on a clean coverslip with roughness of 1-2 nm for spin-coating, a sample

with an average distribution density of single $NaNbO_3$ micro/nano-crystals was obtained on the coverslip.

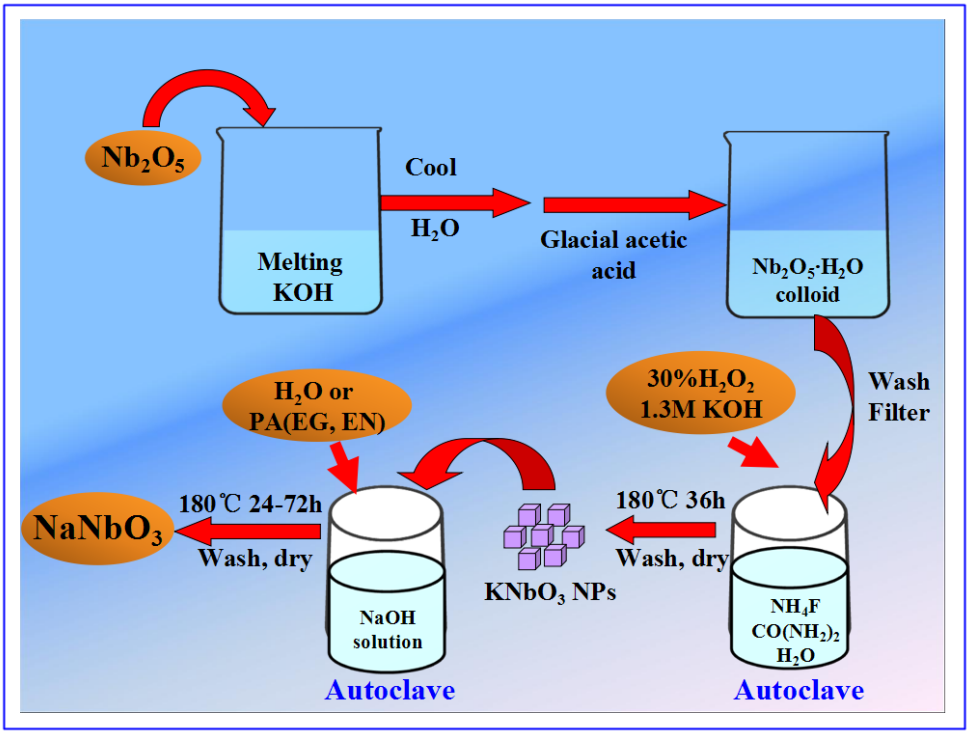

Fig. S1 Flowchart for preparing $NaNbO_3$ micro/nano-crystals by a solution-phase ion exchange route.

Table S1 The experimental parameters of as-prepared $NaNbO_3$ micro/nano-crystals.

Sample No.	KN NPs(g)	NaOH(M)	H_2O(mL)	PA(g)	EG(mL)	EN(mL)	t(h)	T(℃)
No.1	0.12	1.0	20	0	0	0	36	180
No.2	0.12	1.0	20	0.1	0	0	36	180
No.3	0.12	1.0	15	0	5	0	36	180
No.4	0.12	1.0	2	0	18	0	36	180
No.5	0.12	1.0	15	0	0	5	36	180
No.6	0.12	1.0	12	0	0	8	36	180

2 The phase analysis of the as-prepared $KNbO_3$ NPs precursor

Fig. S2 shows the XRD pattern of the as-prepared $KNbO_3$ NPs precursor. Although it cannot be indexed into any XRD pattern presented in Joint Committee on Powder Diffraction Standards (JCPDS) cards, it is completely identical to cubic $K_2Ta_2O_6$ phase (JCPDS Card No. 35-1464, space group: *Fd-3m*, $a = b = c = 1.0596$ nm), indicating that these niobate samples have the same cubic crystal structure as $K_2Ta_2O_6$. The EDS spectrum of products is illustrated in the inset of Fig. S2, the peaks assigned to the designed elements (i.e., K, Nb, and O) are clearly observed and no other impurity is detected. The EDS spectroscopic analysis indicates that the sample mainly consists of K, Nb, and O elements. Therefore, this compound may be a new-phase potassium niobate.

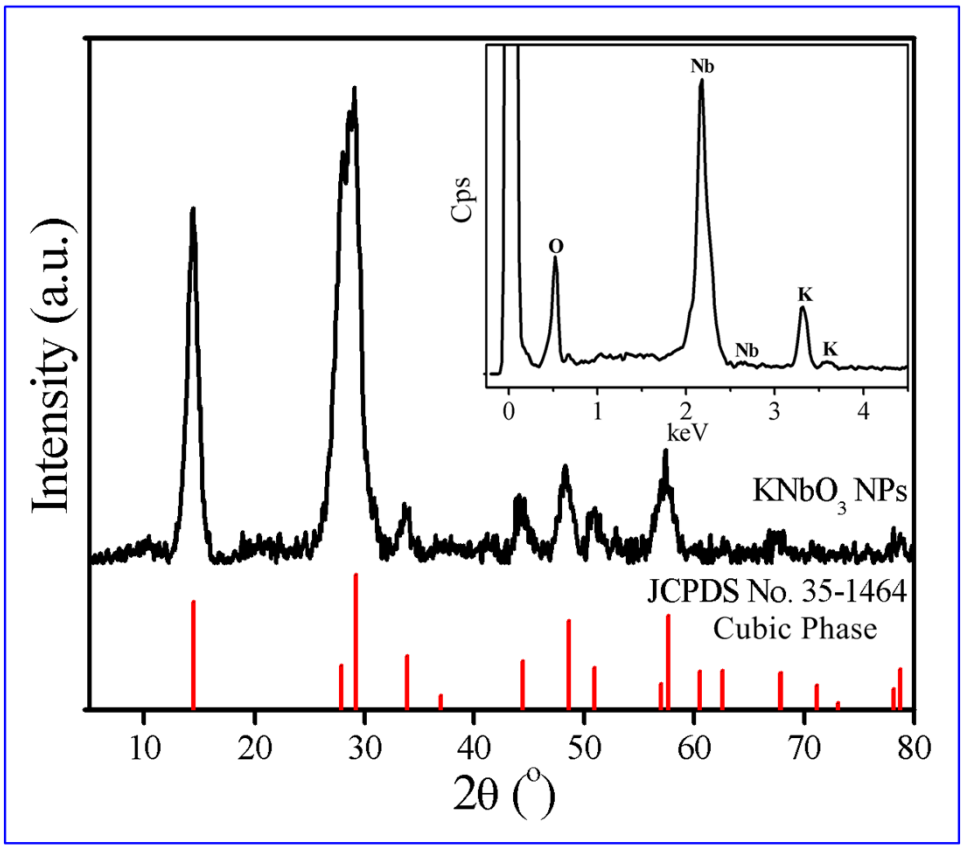

Fig. S2 XRD pattern of the as-prepared $KNbO_3$ NPs precursor, showing the resemblance of the crystal structure with $K_2Ta_2O_6$ (JCPDS Card No. 35-1464). The inset is the EDS analysis of the sample.

3 The morphology analysis of the as-prepared $KNbO_3$ NPs precursor

From the TEM image in Fig. S3a, it is observed that these products are cubic structure with a size of ~ 10 nm.

The HR-TEM image of a single nanoparticle is illustrated in Fig. S3b. The HR-TEM image includes a series of crystal facets with a spacing *d* values of ~0.615 nm, which corresponds to the (111) crystal facet of the cubic phase $K_2Ta_2O_6$ (JCPDS Card No. 35-1464). The SAED pattern corresponding to the $KNbO_3$ NPs is shown in Fig. S3c. Thus these results indicate that the as-prepared $KNbO_3$ NPs with a size of ~10 nm are similar to the cubic phase $K_2Ta_2O_6$ (JCPDS Card No. 35-1464).

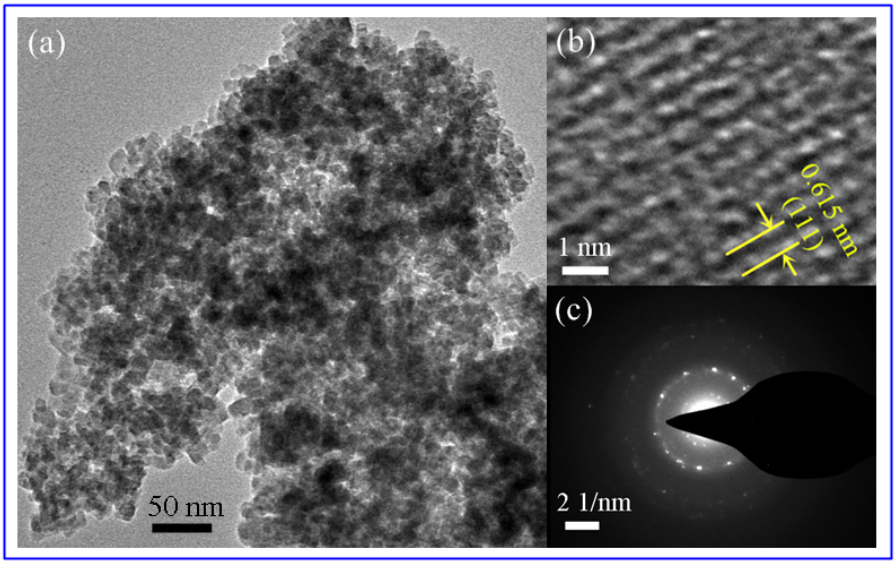

Fig. S3 (a) TEM image and (b) HR-TEM image of the as-prepared $KNbO_3$ NPs precursor, and the scale bar is 50 nm and 1 nm, respectively. (c) SAED pattern of the $KNbO_3$ NPs in (b), and the scale bar is 2 1/nm.

4 The morphology analysis of the as-prepared $NaNbO_3$ micro/nano-crystals

The SEM, TEM, HRTEM and SAED images of as-prepared $NaNbO_3$ micro/nano-crystals are shown in Fig. S4. As shown in Fig. S4, it can be seen that all six samples exhibit relatively uniform, well-dispersed morphologies within micro/nano-size range. Yet the kinds of specific sizes and morphologies of the samples prepared with different preparation conditions are quite different. The distinctions change of size and morphology of the samples is derived from using surfactant or under different reaction mediums, since it is the only difference during the synthesis process.

For the sample prepared in pure distilled water without any surfactant (sample No.1 in Fig. S4a), uniform and

well-dispersed nanowires with ~270 nm in width and ~25 μm in length is obtained. The HR-TEM image in Fig. S4b demonstrates three kinds of crystal lattice fringes with the spacing *d* values of ~0.420, ~0.295 and ~0.260 nm, which corresponds to the (101), (104) and (110) crystal facets of the hexagonal phase $NaNbO_3$ (JCPDS Card No. 37-1076), respectively. The SAED pattern in Fig. S4c indicates that the individual nanowire exhibits a single crystalline character. For the sample prepared in pure distilled water using PA as a surfactant (sample No.2 in Fig. S4d), the sample No.2 presents uniform and well-dispersed regular hexagonal microplates with a size of ~ 6 μm. For the sample prepared in EG-water system with the volume ratio of 1:3 (sample No.3 in Fig. S4e), the sample No.3 presents uniform and well-dispersed irregular cubic nanoparticles with a size of ~ 60 nm. The HR-TEM image and SAED pattern of a single $NaNbO_3$ nanoparticle are illustrated in Fig. S4f and g, respectively. The HR-TEM image demonstrates two kinds of crystal lattice fringes with the spacing *d* values of ~0.528 and ~0.450 nm, which corresponds to the (003) and (101) crystal facets of the hexagonal phase $NaNbO_3$ (JCPDS Card No. 37-1076), respectively. For the sample prepared in EG-water system with the volume ratio of 9:1 (sample No.4 in Fig. S4h and i), uniform and well-dispersed irregular polyhedral nanoparticle with a size of ~ 2.5 μm is obtained. For the sample prepared in EN-water system with the volume ratio of 1:3 (sample No.5 in Fig. S4j), uniform and well-dispersed nanorods with ~360 nm in width and ~8 μm in length is obtained. The TEM images of a single $NaNbO_3$ nanorod are illustrated in Fig. S4k and l, it demonstrates that a nanorod is composed of a bundle of nanowires with ~120 nm in width. And several visible lattice fringes can be observed on the part of a single nanowire in the inset of Fig. S4k, indicating that the nanowires are structurally uniform and may be described as single crystals. For the sample prepared in EN-water system with the volume ratio of 2:3 (sample No.6 in Fig. S4m and n), uniform and well-dispersed regular cubic nanoparticles with a size of ~ 630 nm is obtained. Our results confirm that the surfactant, and reaction medium (water, ethylene glycol/water, ethylenediamine/water) have crucial influences on the crystallization of $NaNbO_3$ micro/nano-structures.

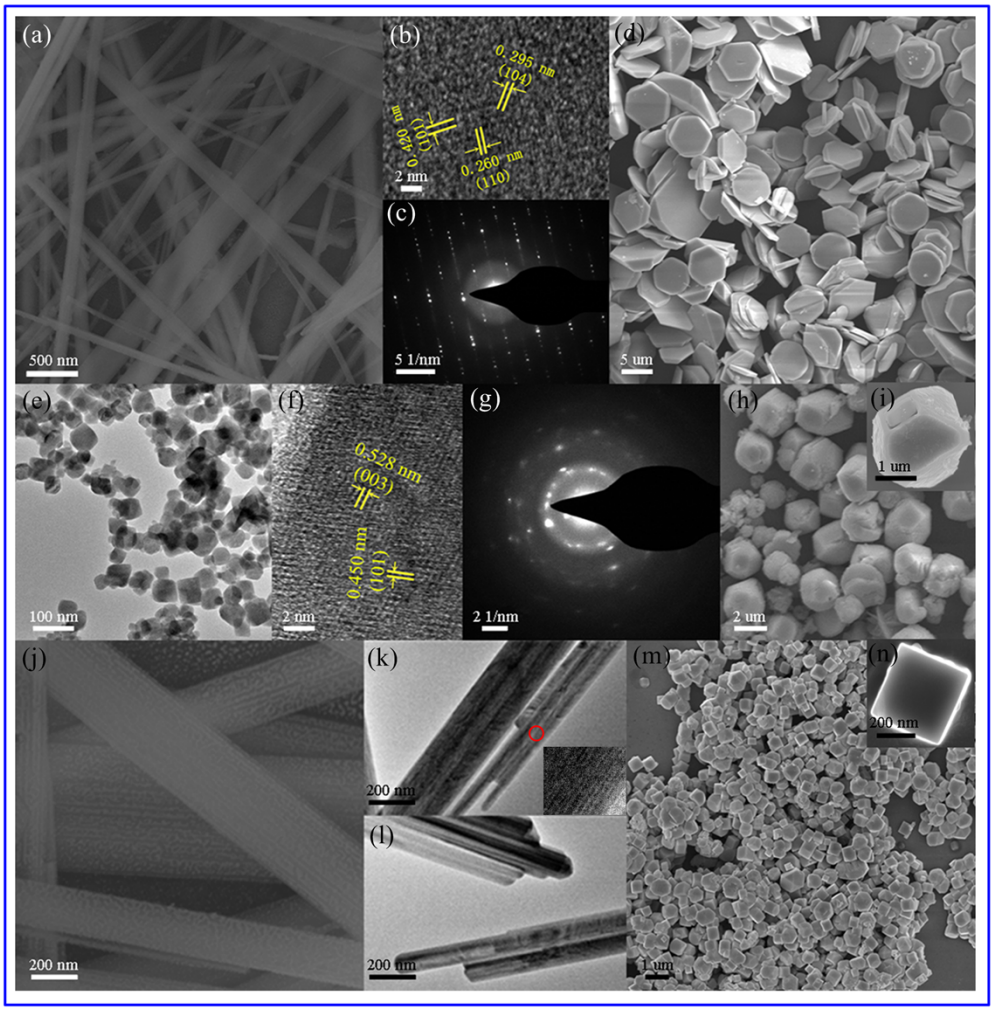

Fig. S4 SEM, TEM, HRTEM and SAED images of the as-prepared $NaNbO_3$ micro/nano-crystals (samples No.1 to No.6). (a, b, c) SEM, HRTEM and SAED images of sample No.1. (d) SEM image of sample No.2. (e, f, g) TEM, HRTEM and SAED images of sample No.3. (h, i) SEM image of sample No.4. (j, k, l) TEM, and HRTEM images of sample No.5. (m, n) SEM image of sample No.6.

5 The EDS analysis of the sample No.4

The XRD pattern of the sample No.4 indicates that these diffraction peaks are consistent with those of the $KNbO_3$ NPs precursor ($K_2Ta_2O_6$: JCPDS Card No. 35-1464). Fig. S5 is the EDS analysis of the sample No.4. The EDS data exhibits the presence of Na, Nb, and O elements, and no K peak can be detected. The results confirmed that an obvious phase transformation from hexagonal to cubic happens when further increase the EG content in EG-water system with the volume ratio of 9:1. K^+ could be completely exchanged by Na^+ via an *in situ*

transformation and recrystallization without changing the original crystal phase.

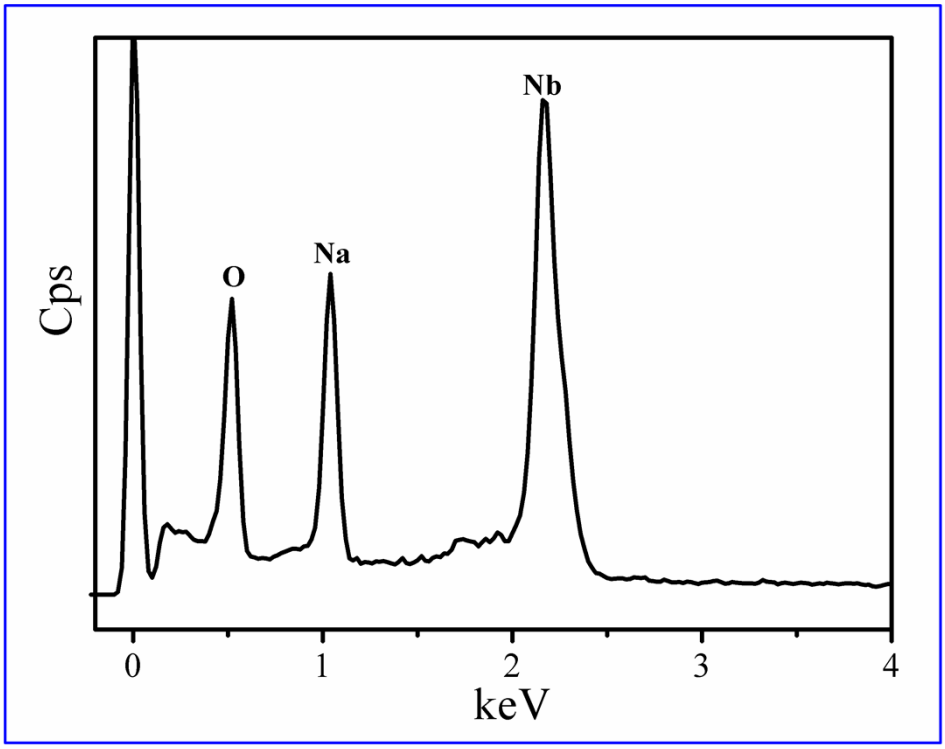

Fig. S5 The EDS analysis of the sample No.4. The EDS spectroscopic analysis indicates that the sample No.4 mainly consists of Na, Nb, and O elements.

6 The growth mechanism of $NaNbO_3$ micro/nano-crystals

The schematic diagram showing the growth mechanism of $NaNbO_3$ micro/nano-crystals (sample No.1 to No.6) is shown in Fig. S6. When the $KNbO_3$ NPs precursor are treated with NaOH aqueous solution, K^+ ions will be released, followed by the Na^+ ions occupying those K^+ vacancies, resulted in a structural collapse.[1] Then a large number of the resultant Nb-O species exist in the alkaline solution system, and their chemical interactions with plenty of Na^+ ions induce the subsequent phase transformation process, which dominates the recrystallization of the hexagonal phase $NaNbO_3$ (sample No.1). If want to fully reveal the details of the mechanism behind this spontaneous process, more work is required in detail. The further growth and morphology evolution of $NaNbO_3$ may be facilitated through Ostwald ripening.[2] The size and shape of $NaNbO_3$ crystals are different from samples No.2 to No.6 owing to the different crystallization rates, which depend on the competition between crystal

nucleation (stage Ⅰ: Nb-O coordinating) and growth (stage Ⅱ: the surface of primary particles adsorbing).

For sample No.2, the organic macromolecules PA accelerate the dissolution of the $KNbO_3$ NPs precursor and the growth of $NaNbO_3$. The water-soluble long-chain PA molecules with many side function groups may promote the transport of Nb-O species towards the growth interface by the clustering of multimers formed in alkaline solution.[3] In order to minimize their surface area, colloidal nanoparticles further coagulate with the assistance of PA, thus inducing the subsequent faster $NaNbO_3$ crystallization. The balance of the dynamic experimental growth conditions is destroyed by introducing the PA molecules, and they also play their roles in the ripening process by face-selective adsorption, making the preferentially growth direction of the hexagonal phase is suppressed and the shape of $NaNbO_3$ particles is controlled. Therefore, PA is dynamically beneficial to the morphology- and phase-controlled crystallization of $NaNbO_3$ particles.

In an EG-water system, it is related to the viscous factors of the solvents and the capping effect. EG is a neutral solvent with two OH^- bonds, and can dissolve polar and ionic substances. The structure enables it to form chelating complexes with metal cations, and thus EG is an ideal capping solvent for the crystallization of metal oxides. In the EG-water system containing 5 mL EG, the nucleation rate of $NaNbO_3$ crystals is greater than its growth rate, thus the uniform and well-dispersed nanoparticles with a size of ~ 60 nm are obtained (sample No.3). In the EG-water system containing 18 mL EG, due to the high concentration of EG brings agglomeration effect, the crystal phase of sample No.4 is consistent with the $KNbO_3$ NPs precursor and the particle size is far greater than No.3.

In EN-water system, the bidentate EN plays two major roles in the growth of $NaNbO_3$ crystals. First, in the case of adding the EN molecules, EN may serve as surface modifiers, inhibiting the axial enlargement of the $NaNbO_3$ crystals.[4] Second, EN would also work as a transport carrier in Ostwald ripening due to its strong chelating ability towards Nb-based species. In a fast ripening process, EN quickly transports growth units by a complexation effect into the growth interface, inducing the $NaNbO_3$ crystals growth rate along the radial direction.

As shown in Fig. S4, when adding the EN molecules, the sample No.5 is shorter than No.1 in length. As compared with No.6, with an increase in the concentration of EN, the morphologies of the $NaNbO_3$ crystals transform initial rod-like structure to the final cubic-like structure and their crystal phases transform hexagonal to cubic. In addition, EN is a strong alkaline solvent, thus making the surfaces of $NaNbO_3$ crystals are very smooth.

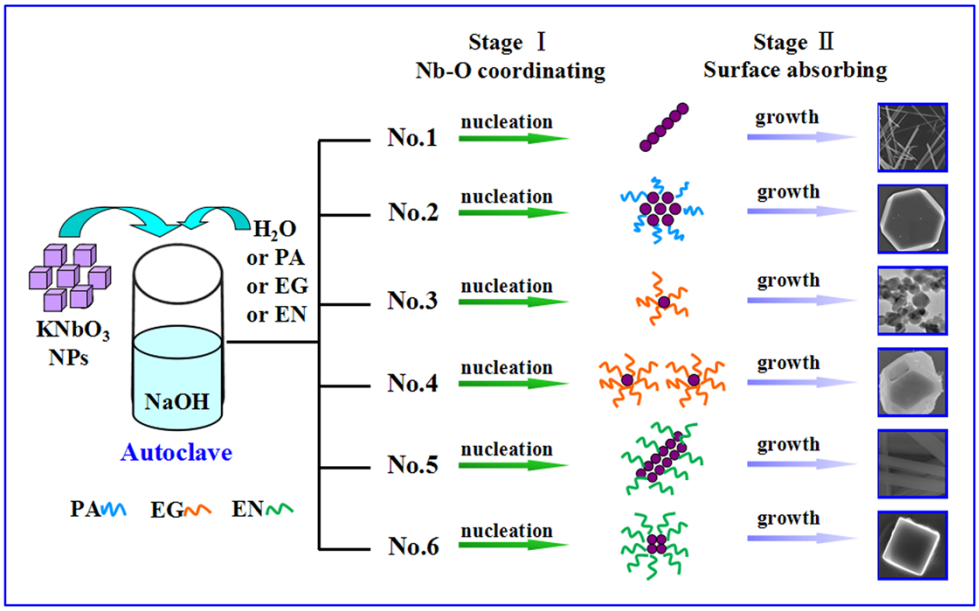

Fig. S6 Schematic diagram showing the formation mechanism of $NaNbO_3$ micro/nano-crystals (samples No.1-No.6).

7 The related derivation of Eq. 2

Transforming from the normal coordinate (x, y, z) to the crystal coordinate (x', y', z'), as shown in Fig. S7.

The relationship of the normal coordinate (x, y, z) and the crystal coordinate (x', y', z'):

$$\begin{bmatrix} E_{x'} \\ E_{y'} \\ E_{z'} \end{bmatrix} = \begin{bmatrix} \cos\psi\cos\varphi - \cos\theta\sin\psi\sin\varphi & \sin\psi\cos\varphi + \cos\theta\cos\psi\sin\varphi & \sin\theta\sin\varphi \\ -\cos\psi\sin\varphi - \cos\theta\sin\psi\cos\varphi & -\sin\psi\sin\varphi + \cos\theta\cos\psi\cos\varphi & \sin\theta\cos\varphi \\ \sin\theta\sin\psi & -\sin\theta\cos\psi & \cos\theta \end{bmatrix} \begin{bmatrix} E_x \\ E_y \\ 0 \end{bmatrix}$$

Eq. (S1)

then, the polarization amplitude vector is given as:

$$\begin{bmatrix} P_{x'} \\ P_{y'} \\ P_{z'} \end{bmatrix} = \begin{bmatrix} 0 & 0 & 0 & 0 & d_{31} & 0 \\ 0 & d_{22} & 0 & 0 & 0 & 0 \\ d_{31} & 0 & d_{33} & 0 & 0 & 0 \end{bmatrix} \begin{bmatrix} E_{x'}^2 & E_{y'}^2 & E_{z'}^2 & 2E_{y'}E_{z'} & 2E_{x'}E_{z'} & 2E_{x'}E_{y'} \end{bmatrix}^T \quad \text{Eq. (S2)}$$

Simplify the above equations, and transform back to the normal coordinate (x, y, z):

$$\begin{bmatrix} E_x^{'} \\ E_y^{'} \\ E_z^{'} \end{bmatrix} \propto \begin{bmatrix} \cos\psi\cos\varphi - \cos\theta\sin\psi\sin\varphi & -\cos\psi\sin\varphi - \cos\theta\sin\psi\cos\varphi & \sin\theta\sin\psi \\ \sin\psi\cos\varphi + \cos\theta\cos\psi\sin\varphi & -\sin\psi\sin\varphi + \cos\theta\cos\psi\cos\varphi & -\sin\theta\cos\psi \\ \sin\theta\sin\varphi & \sin\theta\cos\varphi & \cos\theta \end{bmatrix} \begin{bmatrix} 2d_{31}E_{x'}E_{z'} \\ d_{22}E_{y'}^2 \\ d_{31}E_{x'}^2 + d_{33}E_{z'}^2 \end{bmatrix}$$

Eq. (S3)

The detected light intensity in this paper is considered as $I \propto \left|E_x^{'}\right|^2$, after passing throngh the wave plates, which could be directly achieved by solving Eq. (S3). Firstly, $E_x^{'}$ has been put into the form:

$$E_x^{'} = AE_x^2 + BE_y^2 + CE_xE_y \quad \text{Eq. (S4)}$$

in which

$$\begin{aligned} A = {} & 2d_{31}\left(\cos\psi\cos\varphi - \cos\theta\sin\psi\sin\varphi\right)^2 \sin\theta\sin\psi - d_{22}\left(\cos\psi\sin\varphi + \cos\theta\sin\psi\cos\varphi\right) \\ & \times\left(\cos\psi\sin\varphi + \cos\theta\sin\psi\cos\varphi\right)^2 + d_{31}\sin\psi\sin\theta\left(\cos\psi\cos\varphi - \cos\theta\sin\psi\sin\varphi\right)^2 \\ & + d_{33}\sin^3\psi\sin^3\theta; \\ B = {} & -2d_{31}\cos\psi\sin\theta\left(\cos\psi\cos\varphi - \cos\theta\sin\psi\sin\varphi\right)\left(\sin\psi\cos\varphi + \cos\theta\cos\psi\sin\varphi\right) \\ & - d_{22}\left(\cos\psi\sin\varphi + \cos\theta\sin\psi\cos\varphi\right)\left(-\sin\psi\sin\varphi + \cos\theta\cos\psi\cos\varphi\right)^2 + d_{31}\sin\psi\sin\theta \\ & \times\left(\sin\psi\cos\varphi + \cos\theta\sin\psi\sin\varphi\right)^2 + d_{33}\sin\psi\cos^2\psi\sin^3\theta \\ C = {} & 2d_{31}\left(\cos\psi\cos\varphi - \cos\theta\sin\psi\sin\varphi\right)\left[\sin\psi\sin\theta\left(\sin\psi\cos\varphi + \cos\theta\cos\psi\sin\varphi\right)\right. \\ & \left. - \cos\psi\sin\theta\left(\cos\psi\cos\varphi - \cos\theta\sin\psi\sin\varphi\right)\right] + 2d_{22}\left(\cos\psi\sin\varphi + \cos\theta\sin\psi\cos\varphi\right)^2 \\ & \times\left(-\sin\psi\sin\varphi + \cos\theta\cos\psi\cos\varphi\right) + 2d_{31}\sin\psi\sin\theta\left(\cos\psi\cos\varphi - \cos\theta\sin\psi\sin\varphi\right) \\ & \times\left(\sin\psi\cos\varphi + \cos\theta\cos\psi\sin\varphi\right) - 2d_{33}\sin^2\psi\cos\psi\sin^3\theta \end{aligned}$$

Consequently, the intensity *I* is given as:

$$I = A^2E_x^4 + B^2E_y^4 + \left(C^2 + 2AB\right)E_x^2E_y^2 + 2ACE_x^3E_y + 2BCE_xE_y^3 \quad \text{Eq. (S5)}$$

While $E_x = E\cos\gamma$, $E_y = E\sin\gamma$, E is the incident field, γ is the excitation polarization angle,

$$I = a*\cos^4\gamma + b*\cos^2\gamma\sin^2\gamma + c\sin^4\gamma + d\cos^3\gamma\sin\gamma + e\cos\gamma\sin^3\gamma \qquad \text{Eq. (S6)}$$

in which $a = A^2E^4$, $b = (C^2 + 2AB)E^4$, $c = B^2E^4$, $d = 2ACE^4$, $e = 2BCE^4$.

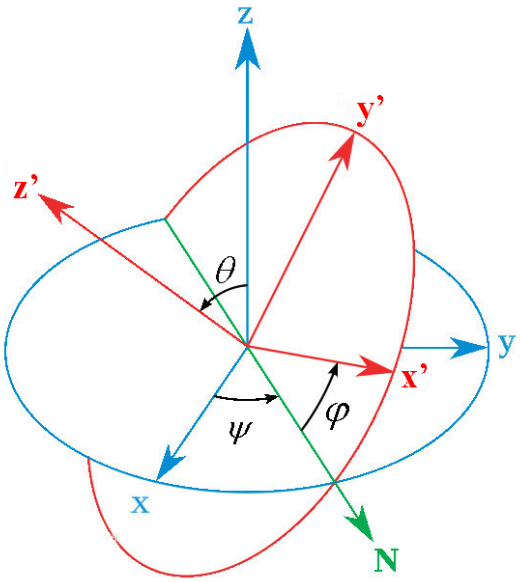

Fig. S7 Schematic diagram of the normal coordinate (x, y, z) and crystal coordinate (x', y', z').

8 References

[1] T. Zhang, Q. Chen and L. Peng, Adv. Funct. Mater., 2008, **18**, 3018.

[2] Y. S. Hu, C. R. Demir, M. M. Titirici, J. O. Müller, , R. Schlogl, M. Antonietti and J. Maier, Angew. Chem. Int. Ed., 2008, **47**, 1645.

[3] M. Mo, J. C. Yu, L. Zhang and S. K. A. Li, Adv. Mater., 2005, **17**, 756.

[4] Y. Liu, Y. Chu, L. L. Li, L. H. Dong, and Y. J. Zhuo, Chem. Eur. J., 2007, **13**, 6667.